Physics – Uspekhi **67** (10) 988 – 999 (2024)

REVIEWS OF TOPICAL PROBLEMS PACS numbers: **72.40.+w, 78.20.–e, 78.56.–a**

Terahertz probing of topological insulators: photoelectric effects

A V Galeeva, A S Kazakov, D R Khokhlov

DOI: https://doi.org/10.3367/UFNe.2023.12.039610

Contents

Abstract. The paper presents a review of the possibilities offered by the study of photoelectric effects in 3D topological insulators and a number of other topologically nontrivial materials under terahertz radiation excitation. We show that, in some cases, the information about the electronic states obtained by such experiments is unique.

Keywords: terahertz radiation, photoelectric effects, photogalvanic effect, photoelectromagnetic effect, photoconductivity

1. Introduction

During the past 15 years, the physics of topological insulators has been one of the rapidly developing areas of modern solid state physics. In three-dimensional topological insulators (TIs), strong spin-orbit interactions result in inversion of the energy levels corresponding to the conduction band and the valence band in the bulk of the semiconductor. As a consequence, two-dimensional topological electron states necessarily appear on the surface of 3D TIs. These states are characterized by a Dirac spectrum with zero effective mass. Furthermore, the direction of the electron spin is fixed perpendicular to its quasi-momentum, which hinders electron backscattering, at least in theory. The two above circumstances make highly attractive the idea of harnessing electron transport over topological surface electron states in electronic devices.

A V Galeeva [(1)], **A S Kazakov** [(1)], **D R Khokhlov** [(1,2,*)]
[(1)] Lomonosov Moscow State University, Faculty of Physics, Leninskie gory 1, str. 2, 119991 Moscow, Russian Federation
[(2)] Lebedev Physical Institute, Russian Academy of Sciences, Leninskii prosp. 53, 119991 Moscow, Russian Federation
E-mail: [(*)] khokhlov@mig.phys.msu.ru

Received 16 October 2023, revised 20 November 2023
Uspekhi Fizicheskikh Nauk **194** (10) 1046 – 1058 (2024)
Translated by E N Ragozin

The existence of topological surface electron states was first confirmed experimentally using angle-resolved photoemission spectroscopy (ARPES) [1]. However, this method does not provide direct information on electron transport. At the same time, transport measurements are fraught with significant difficulties, since topological insulators are usually narrow-gap semiconductors with a large number of electrically active growth defects that form resonant donor or acceptor levels generating a high density of charge carriers that do not freeze out at low temperatures. As a result, the bulk conductivity shunts the conductivity along a thin surface topological layer. Isolating the contribution of surface conductivity is an intricate problem that does not always have an unambiguous solution.

Another experimental approach involves optoelectronic probing of surface electron states. In many cases, photoelectric effects are insensitive to bulk conductivity, even if the free carrier density is high.

It is significant that the characteristic energies of the electron spectrum of topological insulators are low, ranging from units to two to three hundred meV and corresponding to the terahertz spectral range. Therefore, terahertz probing of topological insulators is of special interest.

In this review, we provide examples of photoelectric effects observed during terahertz probing of topological insulators and show that this tool is highly effective in studying the electronic properties of this class of materials.

2. Photogalvanic effects

To study Dirac fermion systems, currently, recourse is actively made to methods based on nonlinear photoelectric effects for which the magnitude of photoinduced currents is proportional to the square of the electric field strength E of the incident electromagnetic wave. One such effect is the photogalvanic effect (PGE), which consists of the occurrence of a photoinduced current in spatially homogeneous systems without an inversion center when exposed to radiation. Linear and circular PGEs are distinguished.

The linear PGE consists of the appearance of a photocurrent induced by linearly polarized incident radiation [2, 3].

The nature of this effect is directly related to the anisotropy of scattering processes. The photocurrent caused by circular PGE is proportional to the degree of circular polarization of radiation [4–6]. The manifestation of the circular effect is related to the asymmetry of the distribution of carrier quasi-momenta in reciprocal space.

The PGE can manifest itself only in systems without an inversion center [7]. Most 3D topological insulators, in particular Bi and Sb chalcogenides, are centrosymmetric in the bulk, but, on the surface, where topological states are formed, the symmetry is reduced and the inversion center is absent, which underlies the selective surface sensitivity of experimental methods for studying PGE-based electron transport. Both linear and circular PGEs are actively studied in various three-dimensional topological insulators [8–15].

2.1 Photogalvanic effects in topological insulators based on $(Bi, Sb)_2Te_3$

Bi- and Sb-based compounds were among the first to be classified as 3D topological insulators [16]. Specifically, $Bi_{1-x}Sb_x$ was the first 3D TI compound experimentally discovered with angle-resolved photoelectron spectroscopy [1]. More recently, calculations were performed in Ref. [17] indicating that Bi_2Te_3, Bi_2Se_3, and Sb_2Te_3 compounds belong to the class of 3D topological insulators. Experimental confirmation of the formation of surface conducting states, wherein the carriers are characterized by the linear Dirac dispersion relation, in the above-mentioned compounds was made in Refs [18–20]. Note that all of the above-mentioned compounds have sufficiently high bulk charge carrier densities up to $n \sim 10^{19}$ cm^{-3} at $T = 4.2$ K, which necessitates the use of surface-selective research techniques.

The crystal lattice of Bi- and Sb-based chalcogenide bulk compounds is characterized by the D_{3d} point group symmetry in the bulk and is centrosymmetric, whereas the surface of such materials has a point group symmetry C_{3v} that is different from the bulk and, therefore, is the only possible region for the manifestation of the PGE.

The photogalvanic effect in bismuth- and antimony-based chalcogenide compounds has been studied in sufficient detail in Refs [9–13]. In a series of studies, heterostructures grown by molecular beam epitaxy were investigated under terahertz photoexcitation conditions employing different laser radiation sources at room temperature.

Figure 1 shows the typical dependence of the normalized amplitude of the linear PGE on the polarization angle of terahertz radiation incident normally onto the sample surface.

The measurements were carried out at two different values of the angle of incidence, $\theta = 0$ and $\theta = 180°$, in order to exclude from consideration another nonlinear photoelectric effect: the photon drag effect, which depends on the direction of the photon momentum and occurs both on the surface and in the volume of centrosymmetric topological insulators. It was experimentally demonstrated that it is precisely the PGE that makes the decisive contribution to the photoresponse.

The origination mechanism of linear PGE is as follows. Incident terahertz radiation results in alignment of charge carrier momenta along the direction of polarization of the electric field. Due to the presence of identically oriented trigonal scatterers on the surface of Bi and Sb chalcogenides, the motion of scattered charge carriers is anisotropic, meaning the emergence of photoinduced current [7].

The linear PGE observed in bismuth and antimony telluride-based compounds at normal incidence of photoexciting terahertz radiation, whose characteristic photon energy is significantly lower than the Fermi energy, can be described with a semiclassical approach. In this case, the Drude radiation absorption by free charge carriers dominates interband optical transitions, and the photogalvanic effect occurs due to the asymmetric scattering of surface charge carriers in the absence of an inversion center on the surface.

In the region of relatively low energy (below 100 meV), satisfying the relation $\omega\tau \gg 1$, where $\omega = 2\pi f$ is the cyclic radiation frequency and τ is the scattering time, the PGE amplitude in Bi- and Sb-based chalcogenide compounds depends on the frequency as follows (Fig. 2):

$$A(f) \propto \frac{1}{1 + (2\pi f\tau)^2}. \qquad (1)$$

Features of the power dependences of some structures in the higher energy region are associated with the activation of interband optical transitions.

The dependences presented make it possible to estimate the main transport characteristics of charge carriers in the near-surface regions using the corresponding relationships for photocurrent and Drude conductivity.

The values of the Fermi energy E_F, the Fermi velocity v_F, and the lifetime of near-surface charge carriers τ and their mobility μ, which were determined from the experimental

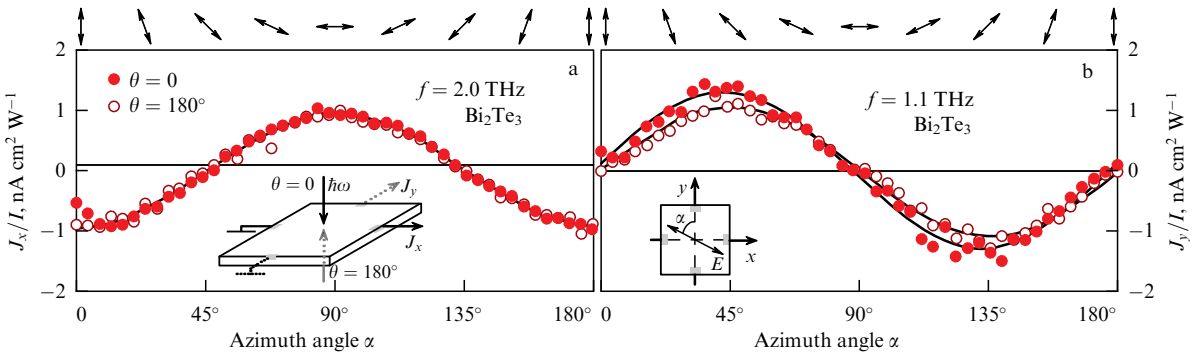

Figure 1. Dependence of ratio of photoinduced current J_x to radiation intensity I on azimuth angle α of polarization plane. Incident radiation frequency: $f = 2$ THz (a) and $f = 1.1$ THz (b). Red dots correspond to angle of radiation incidence $\theta = 0$ and red circles to $\theta = 180°$ [12]. Ratio J_x/I is normalized to maximum value.

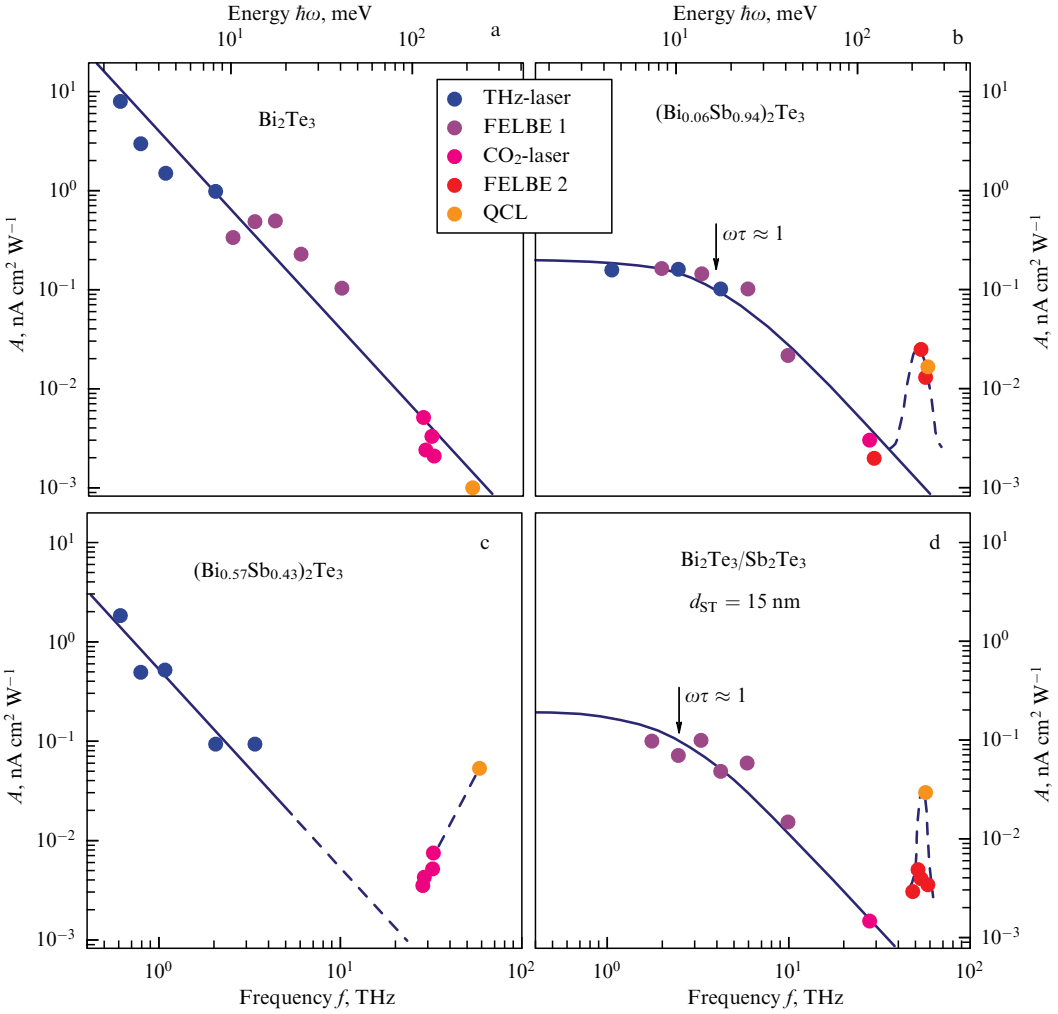

Figure 2. Frequency dependence of ratio of surface photocurrent to radiation intensity in heterostructures based on (a) Bi_2Te_3, (b) $(Bi_{0.06}Sb_{0.94})_2Te_3$, (c) $(Bi_{0.57}Sb_{0.43})_2Te_3$, (d) Bi_2Te_3/Sb_2Te_3 with layer thickness of Sb_2Te_3 $d_{ST} = 15$ nm. Dependence is normalized to maximum value. Different colors of points correspond to different sources of terahertz radiation: optically pumped molecular terahertz laser (THz laser), free-electron laser (FELBE 1,2), quantum cascade laser (QCL), transversely excited carbon dioxide laser (CO_2 laser). Solid lines are plotted using relation (1) [11].

Table. Main transport characteristics of charge carriers in near-surface regions of epitaxial structures based on Bi and Sb tellurides [12].

Sample	Bi_2Te_3	Bi_2Te_3/Sb_2Te_3		$(Bi_{1-x}Sb_x)_2Te_3$	
		$d_{ST}=7.5$ nm	$d_{ST}=15$ nm	$x = 0.43$	$x = 0.94$
E_F, meV	500	140	30	500	7
v_F, 10^5 m s^{-1}	4.3	5.2	2.2	5.1	3.8
τ, ps	> 0.25	0.06	0.06	> 0.25	0.04
μ, cm^2 (V s)$^{-1}$	> 940	1230	1030	> 1330	8210

dependences in compounds studied at room temperature, are collected in the Table.

Under conditions of oblique incidence of an electromagnetic wave on the surface of a 3D Bi- and Sb-based topological phase, also observed was a circular PGE in addition to the linear one [11–13]. The total photoinduced currents measured for two different circular polarizations — right and left — differed due to the presence of a contribution from the circular PGE, which depends on the sign of circular polarization (Fig. 3).

Danilov et al. [13] proposed a phenomenological model whereby the total photocurrent is presented as a superposition of linear and circular contributions:

$$j = j^{\mathrm{circ}} + j^{\mathrm{lin}} . \tag{2}$$

The density of the photoinduced current caused by the circular PGE is given by the following expression:

$$j^{\mathrm{circ}} = \gamma E_0^2 t_p t_s \sin\theta \sin(2\varphi) , \tag{3}$$

where E_0 is the amplitude of the incident wave; θ is the angle of incidence normalized to the refractive index; t_p and t_s are the amplitude transmittances; and φ is the angle of rotation of the $\lambda/4$ plate, which determines the radiation polarization.

The authors of Refs [11–13] associate the observed circular photogalvanic effect with photoionization of surface topological states. The microscopic nature of the effect is based on selective photoexcitation of spin-polarized carriers of two different branches of topological surface states by radiation with the corresponding sign of circular polarization, in accordance with selection rules.

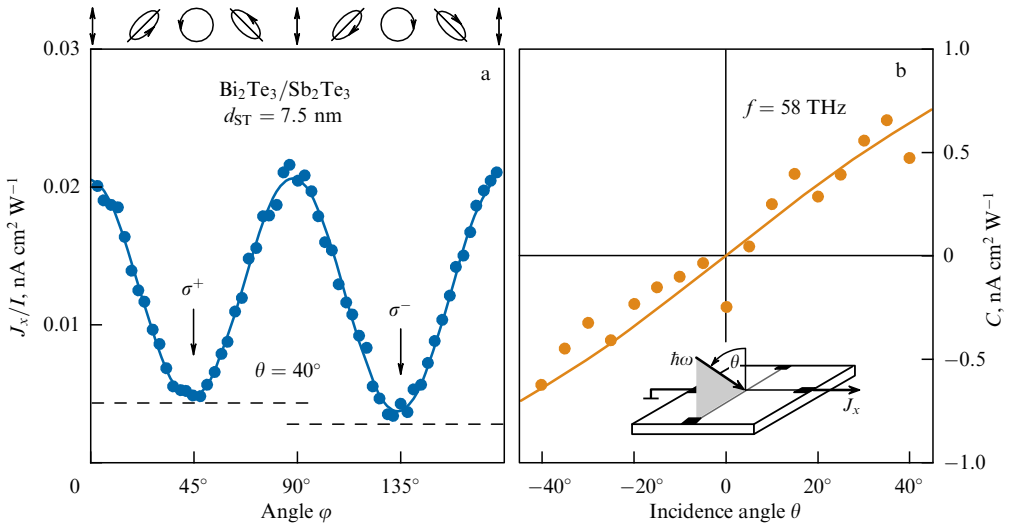

Figure 3. (a) Dependence of photoinduced current on polarization of incident radiation, determined by rotation angle φ of $\lambda/4$ plate. θ is angle of incidence of laser beam. (b) Dependence of normalized amplitude of photocurrent, caused by circular PGE, on angle of radiation incidence [12].

2.2 Photogalvanic effects in HeTe-based topological insulators

In structures based on HgTe, depending on the parameters (layer thickness, composition, temperature, etc.), electronic systems with different properties are realized, and, in particular, the formation of topologically nontrivial phases is possible. For example, in HgTe quantum wells of critical thickness $d = d_c \approx 6.5$ nm, Dirac fermions are observed; for a well width $d > d_c$, a two-dimensional topological insulator is realized [21, 22]; with thicknesses of $d \approx 20$ nm, the structure is classified as a two-dimensional semimetal [23]; in strained 3D HgTe layers with thicknesses of $d \sim 100$ nm, the state of a three-dimensional topological insulator is formed [24].

Unlike Bi- and Sb-based compounds, the crystal lattice of HgTe is characterized by the absence of an inversion center in the bulk of the structure, and therefore observation of the PGE, similar in its microscopic nature to photogalvanic effects in Bi_2Te_3- and Sb_2Te_3-based compounds, does not seem possible. However, in both 2D [25] and 3D films [26, 27] of HgTe, a photogalvanic effect is observed, whose microscopic mechanism the authors associate with the scattering asymmetry caused by the application of an external magnetic field.

In Refs [26, 27], photogalvanic effects were investigated in HgTe-based epitaxial films with a thickness of 80–200 nm. Currents photoinduced by terahertz laser radiation in the structures under study manifest themselves only under conditions of application of a nonzero magnetic field, and the authors of the papers attribute their origin to surface topological conducting states due to the following reasons. First, the magnetic field dependences of photoinduced currents under illumination with either linearly or circularly polarized radiation of opposite sign (σ^+ and σ^-) are nonmonotonic and exhibit extrema that coincide with good accuracy with the position of the cyclotron resonance peaks B_{CR1} and B_{CR2}, corresponding to the electron states on the upper and lower faces of the sample (Fig. 4).

Effective masses calculated from the results of cyclotron resonance measurements are in good agreement with theoretical estimates of the effective masses of charge carriers in surface conducting states obtained by the kp method with the inclusion of Bohr–Sommerfeld quantization.

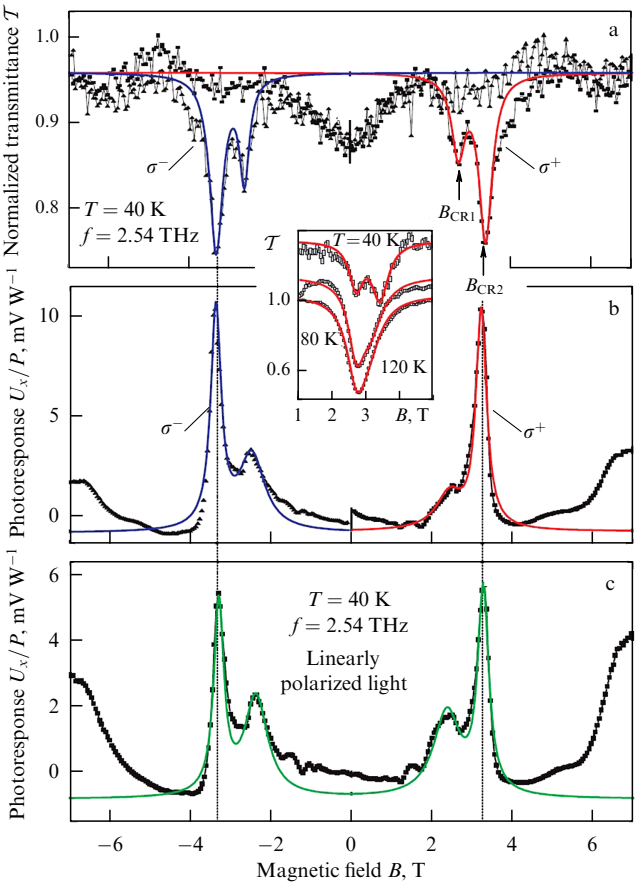

Figure 4. Magnetic-field dependence of transmittance normalized to the maximum (a) and photoresponse per unit power (b, c) in epitaxial 80-nm-thick films based on 3D HgTe measured at $T = 40$ K. Photoresponse was measured under illumination with circular polarization radiation of different signs (b) and under linearly polarized radiation (c). Inset shows averaged magnetic-field dependences of transmittance at different temperatures [26].

Furthermore, measurements performed under conditions of sample rotation relative to the direction of the magnetic field induction vector B by an angle θ showed that the position

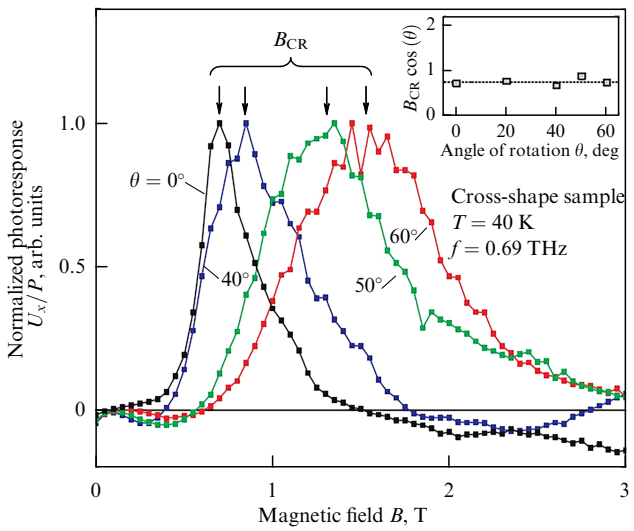

Figure 5. Magnetic-field dependences of normalized-to-its-peak-value photoresponse per unit power measured under conditions of rotation of magnetic induction vector relative to the normal to sample surface by different angles. Inset shows the angular dependence of the projection of the magnetic field B_{CR}, corresponding to cyclotron resonance, on axis normal to sample surface [26].

of the maximum of the magnetic-field dependence of the amplitude of photoinduced current changes according to a cosine law (Fig. 5).

So, the photoinduced current is caused precisely by the magnetic field component normal to the structure surface. This serves as an additional argument in favor of the assumption that the observed photogalvanic effect is closely related to charge carriers in surface two-dimensional electron states.

The authors associate the microscopic nature of the emergence of photoinduced currents with symmetry violation of the scattering of nonequilibrium electrons under the application of an external magnetic field.

The presented results of the PGE investigation in strained 80-nm-thick HgTe films were subsequently used as a reference for studying similar structures with an active layer thickness of 200 nm. The fundamental difference with the latter is at least partial relaxation of the uniaxial lattice stress, which ensures the opening of the energy gap in the bulk.

Experimental results suggest that 200-nm structures contain surface conducting states with similar properties. This is borne out by similar magnetic-field and angular dependences of cyclotron resonance and the amplitude of photoinduced currents in films 200 nm and 80 nm thick, as well as similar effective masses corresponding to surface states.

Finally, investigated in Ref. [28] were photogalvanic effects in epitaxial structures based on solid solutions of $Hg_{1-x}Cd_xTe$ with an active layer thickness of $d \sim 4$ μm. In $Hg_{1-x}Cd_xTe$ alloys, a rearrangement of the band spectrum is possible over a wide range with a change in the Cd_x content, which is accompanied by transition from the topological state ($x < 0.16$) to the trivial state ($x > 0.16$). Despite the absence of an inversion center in the crystal lattice, a circular PGE was observed in the samples of different compositions under study. The authors of the study put forward the following possible reasons for the occurrence of a circular PGE in these compounds. The effect can be associated either with two-dimensional conducting states on the surface of the topological phase of the film or with reduction in the symmetry of the bulk structure. However, the PGE was observed in samples with both a direct ($x > 0.16$) and inverted ($x < 0.16$) energy spectrum, including at room temperature (Fig. 6).

So, the nature of the occurrence of the circular PGE under photoexcitation by terahertz laser radiation in structures based on $Hg_{1-x}Cd_xTe$ solid solutions cannot be associated exclusively with the contribution of charge carriers in two-dimensional topological states. The authors proposed a mechanism for the manifestation of PGE associated with the occurrence of lattice stress, which reduces the symmetry of the bulk crystal.

3. Photoelectromagnetic effect

The photoelectromagnetic (PEM) effect was discovered about 90 years ago [29]. The essence of the effect is the appearance of a voltage drop U_{PEM} across sample contacts oriented perpendicular to the direction of the incident radiation and the magnetic field (Vogt geometry; see the inset in Fig. 7). This occurs due to the emergence of a diffusion flow of photoexcited electrons in a magnetic field by analogy with the Hall effect, in which the electron flow is determined by the applied electric field. The magnitude and sign of the U_{PEM} signal are determined by the magnetic field, as well as the direction and velocity of the carrier diffusion flow. The effect is due to the existence of nonequilibrium photoexcited charge carriers in the surface layer of the semiconductor and can result from photogeneration of excess carriers and from heating of free charge carriers.

The PEM effect was among the important tools for studying the electronic properties of semiconductor materials in the 1960s and 1970s. The main results obtained using this effect in semiconductor physics were summarized in review Ref. [30]. However, in the future, researchers would not pay much attention to the PEM effect, which is apparently due to the explosive growth of interest in low-dimensional semiconductor structures beginning in the 1980s. In such structures, the active layer thickness is significantly smaller than the characteristic diffusion length of nonequilibrium charge carriers, so any noticeable density gradient of the latter at sizes of the order of the structure thickness cannot be observed, and the PEM effect is absent. The photogalvanic effect described in the previous section has a fundamentally different nature, although in a number of external manifestations it is sometimes similar to the PEM effect.

In topological insulators, the thickness of the surface layer in which two-dimensional electron topological states with a Dirac energy spectrum are formed is only about 1–2 nm, which is significantly less than the characteristic diffusion length of nonequilibrium charge carriers in semiconductors. It would therefore seem that the existence of topological surface states in 3D topological insulators cannot entail the appearance of any features of the PEM effect. However, it turned out that this statement is incorrect.

The basis of the experimental approach used in the series of papers [31–34] was the use of a number of solid solutions, for example, $(Bi_{1-x}In_x)_2Se_3$, for which an increase in the content of a lighter element, indium in the case involved, leads to a decrease in the spin-orbit interaction and to a transition of the electron energy spectrum from inverse to direct. Accordingly, the topological phase of the semiconductor

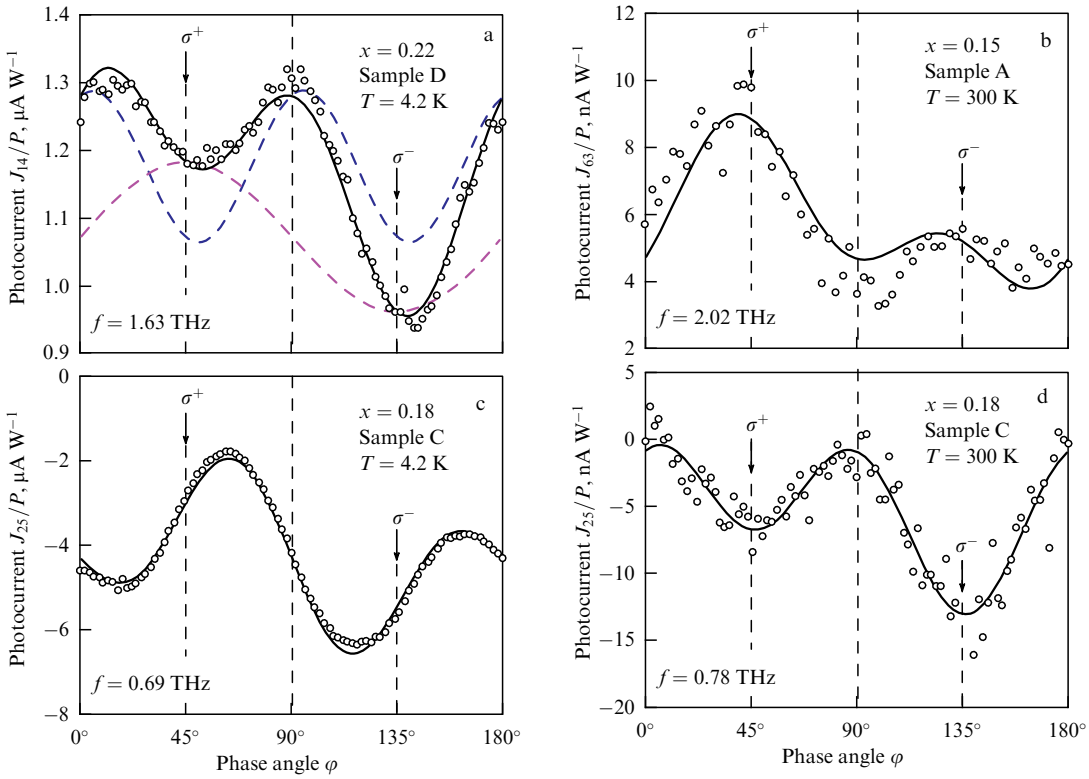

Figure 6. Dependence of photoinduced currents normalized to the power on polarization of terahertz laser radiation with frequencies $f = 1.63$ THz (a), 2.02 THz (b), 0.69 THz (c), and 0.78 THz (d) in samples with compositions $x = 0.22$ (a), 0.15 (b), 0.18 (c, d) at helium (a, c) and room (b, d) temperatures. Solid lines correspond to theoretical estimates. Purple dashed line in panel (a) corresponds to the contribution of circular PGE [28].

changes to the trivial one. The idea of the experiments is to compare the effects observed in different topological states of the solid solutions under consideration.

To excite the PEM effect in Refs [31–34], use was made of laser terahertz radiation. Its photon energy was less than 15 meV and was much lower than the characteristic parameters of the energy spectrum of the semiconductor, such as the energy gap, so the photogeneration of additional free carriers was impossible. Consequently, the effect was entirely due to the heating of charge carriers. In this sense, it is similar to the Nernst effect, wherein the electron temperature gradient is induced by terahertz radiation pulses, and the lattice temperature remains invariable.

We emphasize that the observed effects turned out to be similar for different topologically nontrivial materials: 3D $(Bi_{1-x}In_x)_2Se_3$ topological insulators [31], $Pb_{1-x}Sn_xSe$ [32] and $Pb_{1-x}Sn_xTe$ [34] topological crystalline insulators, as well as Dirac semimetals $(Cd_{1-x}Zn_x)_3As_2$ [33].

The most thorough study was carried out for a system of $(Bi_{1-x}In_x)_2Se_3$ solid solutions [31]. For this system, the transition from the topological to the trivial phase occurs at an In_2Se_3 molar fraction $x = 0.06$. The high density of growth defects leads to a strong degeneracy of the electron gas at low temperatures with a free electron density, as a rule, not lower than $10^{18} - 10^{19}$ cm^{-3}.

It is significant to note that the PEM effect is observed for both topological and trivial phase samples at low temperatures $T < 14$ K. The effect was manifested only in a nonzero magnetic field, and its magnitude was odd with respect to the magnetic field, i.e., the PEM effect voltage changed sign when the magnetic field direction changed. The characteristic dependence of the PEM effect amplitude U_{PEM} on the magnetic field B at $T = 4.2$ K is shown in Fig. 7 for different samples. This type of $U_{PEM}(B)$ dependence is quite characteristic of the PEM effect [30]. It is significant that for all samples the sign of the PEM effect corresponded to the diffusion of charge carriers from the surface into the bulk (see the inset in Fig. 7). Note that, for a given direction of magnetic field, the sign of the PEM effect is uniquely defined by the direction of diffusion of nonequilibrium charge carriers.

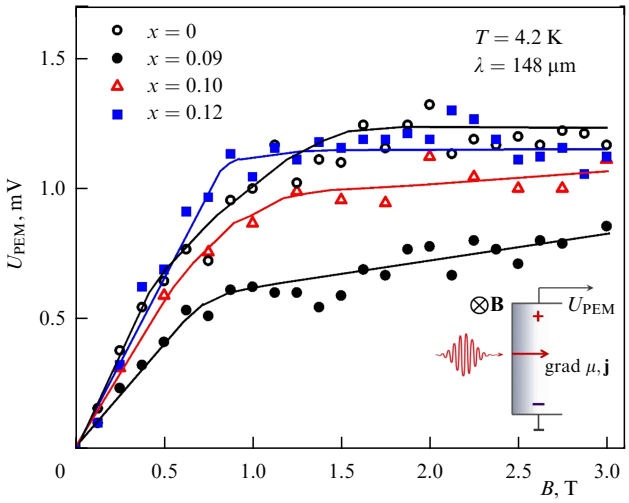

Figure 7. Dependence of amplitude of PEM effect induced by radiation with a wavelength of 148 μm on magnetic field at $T = 4.2$ K for $(Bi_{1-x}In_x)_2Se_3$ samples with different compositions $x = 0$, 0.09, 0.1, 0.12. Inset shows experimental setup [31].

The main idea of the experiment was to compare the features of the PEM effect for samples with the same or

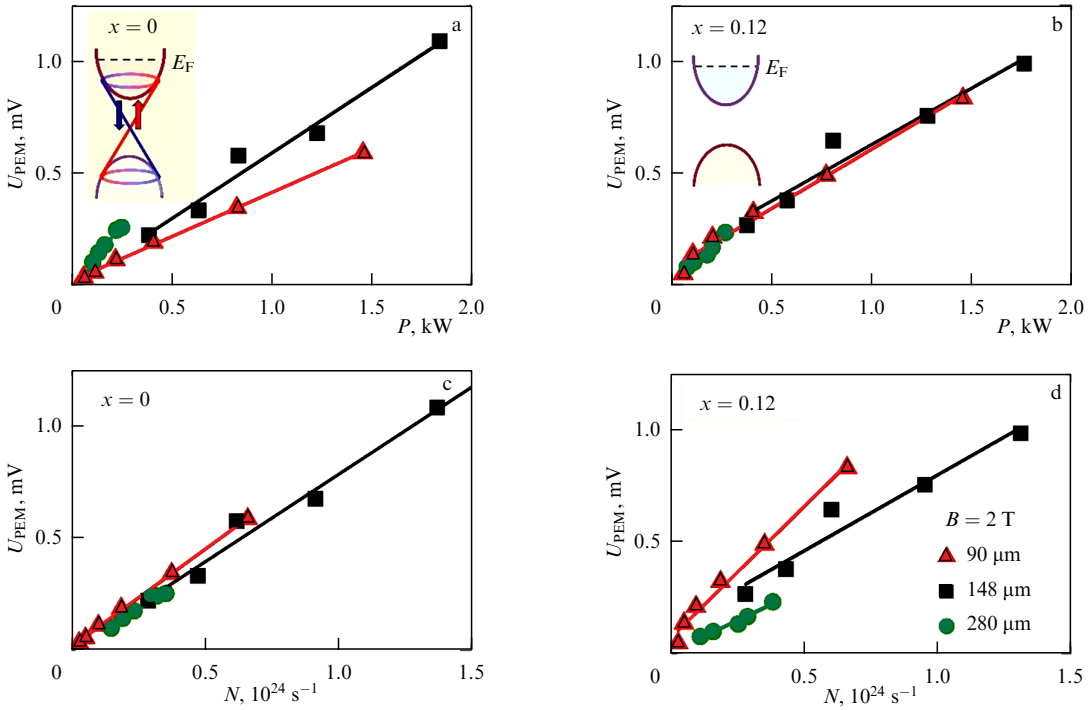

Figure 8. Dependence of amplitude of PEM effect on power (a, b) and the number of photons (c, d) of incident radiation for Bi_2Se_3 (a, c) and $(Bi_{0.88}In_{0.12})_2Se_3$ (b, d) samples. Radiation wavelength was 90, 148, and 280 μm [31].

similar energy gaps and free electron densities but possessing either an inverted or direct electron energy spectrum. Samples with compositions $x = 0$ and $x = 0.12$ best meet this criterion. Figures 8a and 8b show the dependence of the PEM effect amplitude U_{PEM} on the incident radiation power P for different laser wavelengths λ. It is evident that U_{PEM} depends almost linearly on P for a given value of λ both for $x = 0$ and for $x = 0.12$. At the same time, there is a significant difference between the two samples. In the sample with $x = 0.12$, which is in the trivial phase, the amplitude of the PEM effect U_{PEM} is practically independent of the wavelength of the incident laser radiation at a given power P of the radiation, while, for the sample with $x = 0$, which is in the topological phase, U_{PEM} depends on λ. On the contrary, the amplitude of the PEM effect U_{PEM}, calculated as a function of the incident radiation photon flux $N = P\lambda/hc$, does not depend on the laser wavelength λ for the sample with $x = 0$ in the topological phase and depends on it for the sample of the trivial phase with $x = 0.12$ (Figs 8c, 8d).

Since the charge carrier density gradient between the surface and the bulk of the semiconductor is impossible due to the small energy of exciting radiation photons, the only possible reason for the occurrence of an electron diffusion flux from the surface into the bulk of the sample is the difference in the mobility of charge carriers on the surface and in the bulk. If only ordinary band electrons were involved in the effect, such a difference in mobility between hot electrons on the surface and cold electrons in the bulk would not arise, since the electron mobility is saturated at low temperatures. Then, the electron flows from and to the surface would exactly compensate each other, and the effect, would not be observed. Therefore, to observe the effect, it is necessary that there be conducting electron states on the surface of the semiconductor, and their mobility should be higher than the bulk one in order to ensure the diffusion flux of carriers from the surface into the bulk. Since the effect is observed in samples with both an inverse and direct energy spectrum, the very appearance of the PEM effect only indicates the presence of surface electron states with increased mobility, which are not necessarily topological. At the same time, the characteristics of these surface states are significantly different for the topological and trivial phases.

As shown in Ref. [31], the reason for such a difference may lie with the strong suppression of the electron-electron interaction in topological surface electron states compared to the highly mobile surface states of the trivial phase. Then, in samples with an inverse spectrum corresponding to the topological phase, diffusion of photoexcited electrons occurs first, and only later does their thermalization happen. As a result, the signal of the PEM effect is determined by the flux of incident radiation photons. In samples with a direct spectrum, which are in the trivial phase, on the contrary, thermalization occurs first, and only then does diffusion into the sample depth happen, and the signal is determined by incident radiation power.

The suppression of electron-electron interaction in the topological phase is in all likelihood due to the fact that the electron spin direction is tied to the direction of its quasi-momentum, due to which electrons that can effectively interact must have the same quasi-momentum direction. For the trivial phase, there are no such limitations, and the number of electrons that can effectively interact is significantly greater. Accordingly, the characteristic thermalization time of heated charge carriers is shorter.

It is significant that the above effect of different scaling of the amplitude of the PEM effect for the topological and trivial phases is common to different systems of 3D topological insulators [31], topological crystalline insulators [32, 34], and Dirac semimetals [33]. Consequently, the reason for the appearance of such an effect is probably the same and may consist in the suppression of electron-electron scattering in topologically nontrivial electron states.

4. Photoconductivity

As noted above, the majority of topological insulators are narrow-gap semiconductors with a significant number of growth defects, which are usually electrically active. As a result, topological insulators are usually highly degenerate semiconductors with a free carrier density of 10^{18}–10^{19} cm^{-3}. To record photoconductivity on top of a high background equilibrium conductivity provided by such a significant carrier density is a very difficult and, in most cases, practically unsolvable problem.

An exception to the above rule is the system of $Hg_{1-x}Cd_xTe$ solid solutions. As already mentioned above, the rearrangement of the energy spectrum with increasing x in the alloy is accompanied by a transition from the inverse band structure for $x \lesssim 0.16$ to the direct order for $x \gtrsim 0.16$ (Fig. 9). The domain of compositions $x \lesssim 0.16$ corresponds to the topological phase, which is distinguished by the existence of surface states with a Dirac spectrum. Compositions with a direct band structure correspond to the trivial phase. Modern epitaxial growth techniques make it possible to synthesize $Hg_{1-x}Cd_xTe$ films with a high mobility ($\sim 10^5$ cm^2 (V s)$^{-1}$ at $T = 77$ K) and with a low free carrier density of $\sim 10^{14}$ cm^{-3} [35, 36]. This makes it possible to measure the photoconductivity against the background of such a rather low equilibrium carrier density.

Due to the low background charge carrier density and the possibility of varying the band gap over a wide range, $Hg_{1-x}Cd_xTe$ solid solutions with $x \gtrsim 0.2$ and a direct structure of the energy spectrum have found application as base materials for IR photodetectors [37]. Interest in studying terahertz photoelectric phenomena in such objects is due primarily to the need to develop an elemental and component base for optical applications and to expand the working spectral range of optoelectronic devices to the long-wavelength domain. Studies of terahertz photoconductivity in structures based on $Hg_{1-x}Cd_xTe$ solid solutions with $x \gtrsim 0.2$ and a direct structure of energy bands made it possible to establish a number of features of the electronic spectrum caused by the presence of acceptor centers: mercury vacancies [38, 39].

In the topological phase, transport phenomena, both under equilibrium and nonequilibrium conditions, have been investigated to a greater extent in HgTe films. Terahertz probing in combination with the use of different experimental techniques has made it possible to detect the manifestation of topological states in optical properties (Kerr and Faraday effects) [41–43], transport (quantum Hall effect, Shubnikov–de Haas oscillations) [44–48], and photogalvanic effects [25–27, 49].

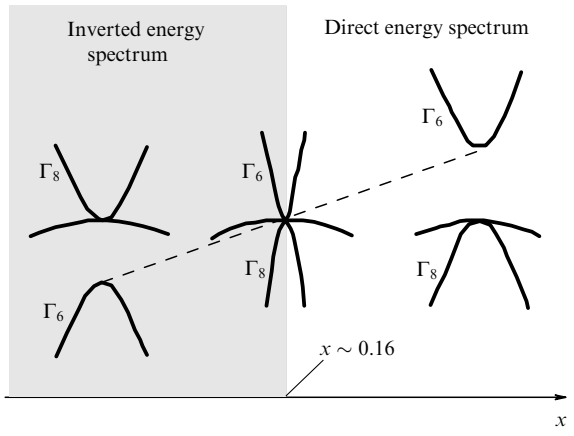

Figure 9. Rearrangement of energy spectrum, represented by electron states with Γ_6 and Γ_8 type symmetries, in the bulk of $Hg_{1-x}Cd_xTe$ solid solutions at zero temperature [40].

Terahertz photoconductivity in a magnetic field in 3D TIs based on strained epitaxial HgTe films was investigated in Ref. [50]. The use of transistor-type structures with a transparent gate as samples made it possible to reveal the special features of nonequilibrium transport with a controlled change in the position of the Fermi level in the allowed bands and against the background of the energy gap. A comparison of the transport properties in the dark and under laser irradiation showed that the observed photoconductivity is due to the heating of the sample by incident radiation. The authors of Ref. [50] recorded a cyclotron resonance associated with photoexcitation in a system of Dirac fermions and determined the dependence of surface carrier cyclotron mass on the position of the Fermi level. The resultant mass values are in good agreement with the theoretical and experimental values for Dirac fermions in HgTe [51, 52]. At high carrier densities in the bulk, MIRO-type magnetoresistance oscillations induced by terahertz radiation were detected in Ref. [50], which were caused by the contribution of a two-dimensional electron gas on the surface [53] (Fig. 10).

In solid solutions in the composition range $x < 0.16$, which corresponds to the topological phase, transport and optoelectronic phenomena have been studied to a lesser extent. It is noteworthy that, as shown by studies of the galvanomagnetic properties of 3D epitaxial layers of $Hg_{1-x}Cd_xTe$ with $x < 0.16$, such objects exhibit the quantum Hall effect as well as other features of magnetotransport, indicating the decisive contribution of surface topological states to the mechanism of electrical transport [47, 54].

In a series of studies [55–62], photoconductivity excited by terahertz laser radiation pulses was investigated in thick $Hg_{1-x}Cd_xTe$ films of different compositions corresponding to both the topological and trivial phases. The samples under study were synthesized by molecular beam epitaxy (MBE) on a semi-insulating GaAs substrate. The equilibrium density of free electrons at liquid helium temperature was less than 10^{15} cm^{-3}, while the Hall mobility was $10^5 - 10^6$ cm^2 V^{-1} s^{-1}, which indicates the high quality of the structures studied. The measurements were carried out at a temperature of $T = 4.2$ K in a magnetic field of up to 3 T. The magnetic field was directed along the normal to the sample surface. The exciting terahertz radiation was also directed perpendicular to the sample surface, i.e., the experiment was conducted in the Faraday geometry.

Experiments have shown that the photoconductivity has different signs for the topological and trivial phases of $Hg_{1-x}Cd_xTe$ in the absence of a magnetic field. For compositions $x > 0.16$, corresponding to the trivial phase, the photoconductivity was negative, and for compositions $x < 0.16$, corresponding to the topological phase, it was positive [40]. Such a noticeable difference was interpreted as follows. The negative photoconductivity observed for the trivial phase samples is due to the heating of free electrons. Since the band gap of the semiconductor is small, the electron dispersion relation differs greatly from the parabolic one and is close to the Kane one. In this case, the effective mass increases linearly with energy, which entails a decrease in the

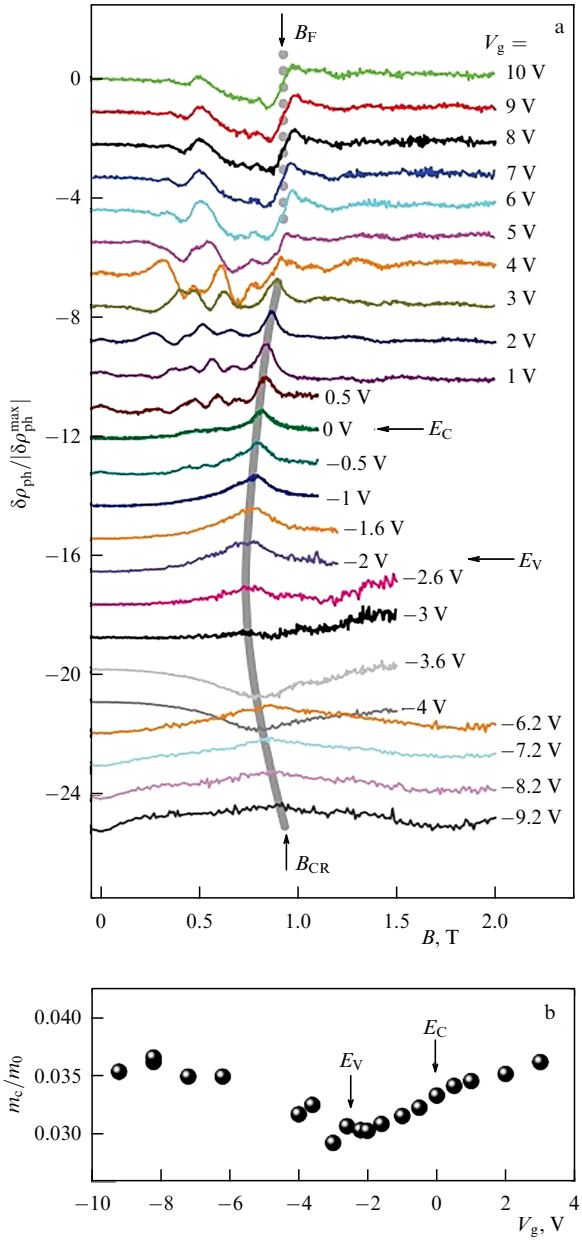

Figure 10. (a) Magnetic-field dependence of photoconductivity (photoresistance) of strained HgTe layers for different positions of Fermi level. Boundaries of allowed bands E_C and E_V, as well as magnetic fields B_{CR} and B_F corresponding to cyclotron resonance and MIRO, are indicated by arrows. Photoresistance is normalized to maximum value. (b) Dependence of cyclotron mass m_c normalized to free electron mass m_0 on gate voltage V_g, which determines position of Fermi level [50].

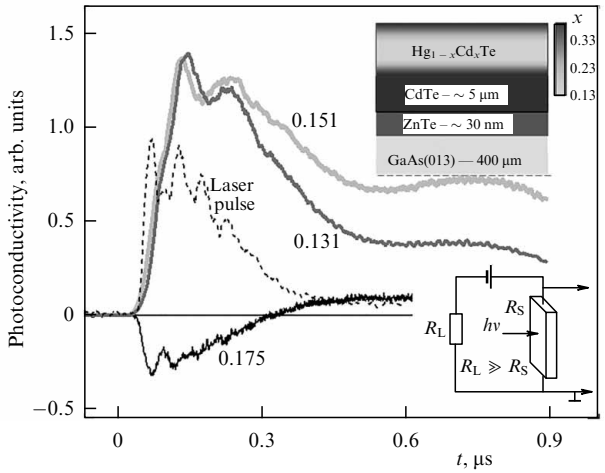

Figure 11. Kinetics of terahertz photoconductivity induced by laser radiation with a frequency of 1.07 THz in $Hg_{1-x}Cd_xTe$ samples of different compositions: $x = 0.131, 0.151, 0.175$. Insets show a schematic image of layers of the epitaxial structure based on $Hg_{1-x}Cd_xTe$ (top) and experimental setup (bottom) [40].

mobility of hot electrons, and negative photoconductivity is observed. A similar effect should be observed in the topological phase samples, but there, in all likelihood, a different mechanism is dominant, leading to positive photoconductivity. The main possible interpretation proposed by the authors of Ref. [55] is as follows. Heating of charge carriers in the film volume leads to diffusion of hot photoexcited electrons into the heterojunction region between the film in the topological phase and the $Hg_{1-x}Cd_xTe$ graded-gap buffer on which it was grown and which corresponds to the trivial phase. According to the theory, two-dimensional topological electron states with a linear dispersion relation and, accordingly, zero effective mass should be formed in this domain. Then, the hot electrons diffusing into this layer acquire increased mobility, which leads to positive photoconductivity.

Even in low magnetic fields $B \sim (0.05-0.1)$ T, the kinetics of photoconductivity become alternating: immediately after the onset of the laser pulse, the photoconductivity is negative, but then it changes sign and becomes positive. The amplitude of the negative part of the photoconductivity is symmetrical relative to the direction of the magnetic field and is also the same for two pairs of potential contacts located on opposite sides of the Hall bridge. The nature of the change in the amplitude of the positive part of the photoconductivity is much more intriguing (Fig. 11).

For one of the magnetic field directions, the amplitude of positive photoconductivity first increases rapidly, reaches a maximum for a field of about 0.07 T, and then rapidly decreases, so that only the negative part of photoconductivity is observed at $B > 1$ T. For the opposite field direction, however, the positive photoconductivity disappears almost immediately, and only the negative photoconductivity is observed. Therefore, positive photoconductivity turns out to be asymmetrical with respect to the magnetic field. Since a change in the magnetic field direction corresponds to the operation of time reversal, the effect described can be interpreted as a violation of the T-symmetry of photoconductivity.

Photoconductivity measurements on two equivalent pairs of potential contacts located on opposite sides of the Hall bar should give identical results in the geometry of the experiment. This is indeed the case in a zero magnetic field, but such equivalence is violated for a nonzero magnetic field (Fig. 12). This effect can be interpreted as a violation of spatial parity, or P-symmetry. At the same time, if we simultaneously replace the pair of contacts with a mirror-image one on the Hall bar and the magnetic field with an oppositely directed one, then the amplitude of positive photoconductivity will not change, i.e., the effect exhibits PT-symmetry.

It is especially significant to note that the equilibrium characteristics, in particular magnetoresistance, are a symmetrical function of the magnetic field and do not differ for mirror-image pairs of contacts. Therefore, the noted asymmetry of properties manifests itself only in a nonequilibrium situation.

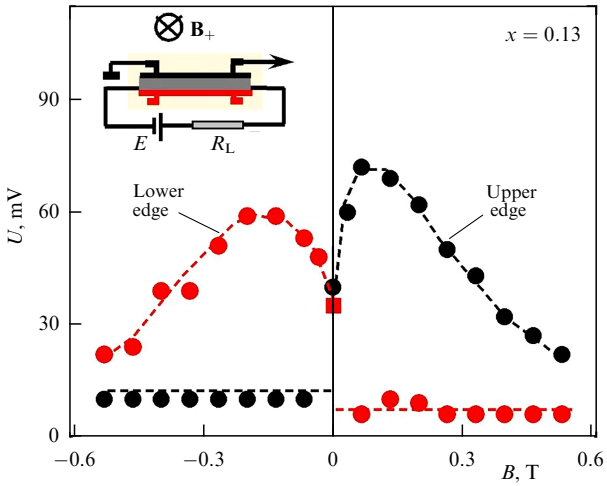

Figure 12. Positive photoresponse induced by 1.07-THz radiation in a magnetic field in a $Hg_{0.87}Cd_{0.13}Te$ sample with inverted energy spectrum. Inset shows experimental setup (adapted from Ref. [56]).

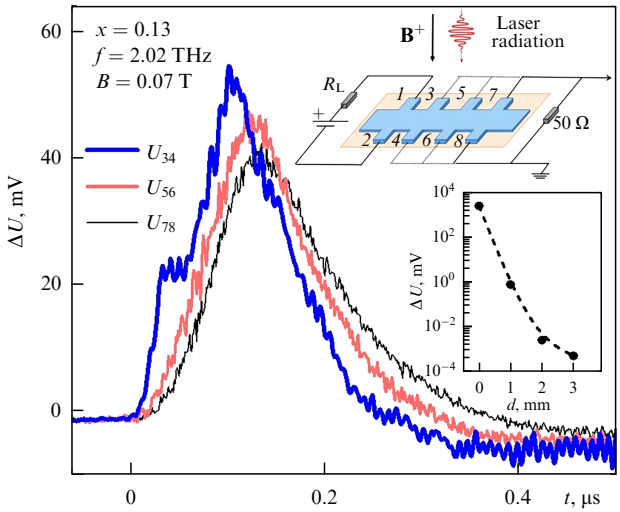

Figure 13. Nonlocal photoresponse kinetics in a magnetic field of 0.07 T under excitation conditions by radiation with a frequency of 2.02 THz in a $Hg_{0.87}Cd_{0.13}Te$-based structure. Photosignal was recorded using different pairs of potential contacts on Hall bar. Insets show experimental setup (top), dependence of voltage across potential contacts on distance between current and potential contacts (bottom) [59].

It is also significant that the effect of photoconductivity asymmetry in a magnetic field was observed in almost all samples corresponding to the topological phase, and only its amplitude changed slightly. In samples corresponding to the trivial phase, the effect was not observed.

It is immediately obvious that the described effect does not correspond to the visual symmetry of the experiment. One might assume that the sample has some 'built-in' nonuniformity, which manifests itself only under nonequilibrium conditions. In this case, the effect should be tied to a certain physical side of the sample and cannot change when the sample is turned 180° about the normal. Experimentally, it turns out that, with such manipulation, the effect does not change in the laboratory coordinate system, i.e., it moves to the opposite physical side of the sample. Consequently, the existence of the effect is due to the action of a factor external to the sample, which reduces the symmetry of the system.

In Ref. [56], several such possibilities were analyzed: deviation of the angle of incidence of radiation from the normal, direction of incidence of radiation from the surface layer side or from the substrate side, presence of a weak component of the magnetic field along or across the Hall bar, and spatial nonuniformity of photoexcitation. It turned out that the effect is stable in all of the above departures of the experimental geometry from the ideal one. The nature of the external factor entailing the emergence of the effect is still unclear.

Since positive photoconductivity is observed only in samples corresponding to the topological phase, it was hypothesized that the effect is associated with specific properties of the two-dimensional layer that makes its appearance at the interface between the topological and trivial phases. It is well known that one of the properties of such a layer may be nonlocal conductivity, when the current flows along the edge of the sample [63]. For nonlocal conductivity, a special experimental geometry is used, for which the current contacts are located away from the potential ones (Fig. 13). The corresponding experiment is described in Ref. [59]. Under equilibrium conditions, the voltage drop across the potential contacts decreases exponentially as they move away from the pair of current contacts, i.e., equilibrium nonlocal conductivity is absent. Nonlocal photoconductivity is also absent in a zero magnetic field, but, when the field is introduced, it turns out to be quite significant (Fig. 13).

Important properties of edge photocurrents are the following. First, the edge photocurrent hardly decreases as the pair of potential contacts is moved away from the current contacts. Second, photocurrents are absent in the absence of applied voltage, and they change sign when the polarity of the voltage changes. Third, edge photocurrents change direction to the opposite one when the polarity of the magnetic field changes. Finally, their most surprising property is chirality: photocurrents flow around the sample along its edge.

As indicated in Ref. [61], the effect of *PT*-symmetric photoconductivity observed in the Hall bar geometry is related to the superposition of traditional photoconductivity over the film volume and chiral nonlocal photoconductivity along its edge. At one edge of the Hall bar, these two contributions are added together, and, at the other, they are subtracted from each other, which results in the observed effect.

Despite the fact that the nature of the unusual photoconductivity observed in thick films based on the topological phase of $Hg_{1-x}Cd_xTe$ remains unclear, it was possible to determine the region of the structure that is a 'reservoir' of nonequilibrium electrons, as well as of the region responsible for the appearance of the effect. To this end, in Ref. [62], the photoconductivity was investigated in structures from which the cadmium telluride cover layer was successively etched, then 1.5 μm and 3 μm of the active layer were successively etched, so that in the thinnest structure the film thickness was about 1 μm. It turned out that the amplitude of the effect increases sharply after etching the cover layer, and then it decreases sharply, and in the thinnest film the effect is not observed. It is inferred that the source of nonequilibrium electrons is the volume of the film, and the place where unusual properties appear is the interface between the film, which is in the topological phase, and the buffer or cover layer, which is in the trivial phase.

Determining the nature of the external factor responsible for the appearance of asymmetric photoconductivity in

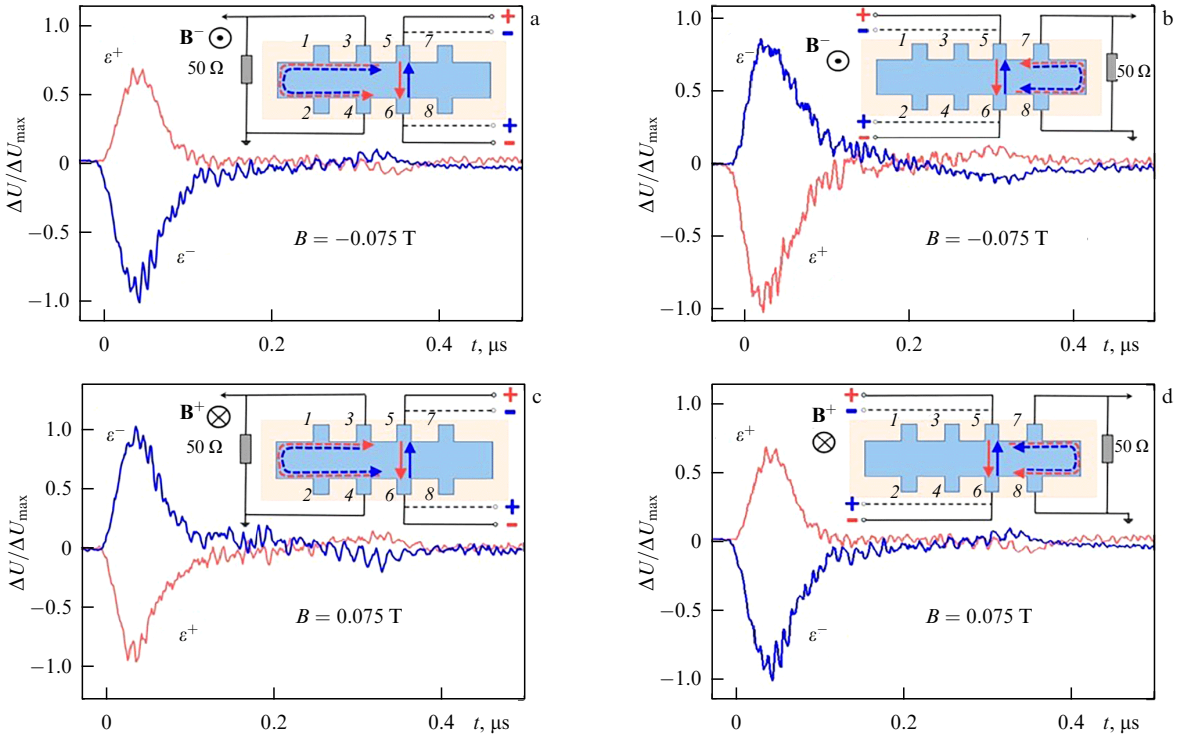

Figure 14. Kinetics of nonlocal photoresponse induced by radiation with frequency $f = 1.07$ THz in a magnetic field of 0.075 T in a $Hg_{0.81}Cd_{0.13}Te$ sample. Photoresponse changes sign both when polarity of bias voltage changes and when polarity of magnetic field changes. Insets a–d show experimental setups; arrows schematically indicate directions of induced currents [59].

structures based on thick $Hg_{1-x}Cd_xTe$ films is a very intriguing task that invites additional research.

5. Conclusions

The results presented in this review suggest that the study of photoelectric phenomena in 3D topological insulators using terahertz probing techniques allows one to observe a number of nontrivial effects, which are largely due to the fundamental difference in the electronic characteristics between the two-dimensional layer on the surface of topological insulators and the bulk of the material.

Among these phenomena are, in particular, linear and circular photogalvanic effects, which occur only in the absence of an inversion center. In topological insulators based on bismuth and antimony chalcogenides, such a situation is realized only on the surface, while the volume is centrosymmetric and, therefore, cannot contribute to the observed effect. This allows us to directly determine a number of key transport characteristics of carriers in the topological conducting layer.

Another example is the difference in the dependence of the amplitude of the photoelectromagnetic effect on the incident terahertz radiation intensity for the topological and trivial phases in structures based on bismuth chalcogenides and their solid solutions. The study of such dependences made it possible to show that the energy relaxation of hot electrons in the topological phase is significantly suppressed compared to the trivial phase.

Lastly, another example of nontrivial photoelectric phenomena in topological insulators is the highly unusual chiral nonlocal terahertz photoconductivity in heterostructures based on $Hg_{1-x}Cd_xTe$ solid solutions. It is shown that the region of localization of the effect is the topological phase–trivial phase heterojunction, in which the emergence of a two-dimensional topological conducting layer is expected.

So, the given examples show the fundamental difference between research based on the study of photoelectric phenomena and, for example, studies of electron transport, in which the volume of the semiconductor makes a significant contribution to the observed effects and extracting the contribution of topological states is difficult and not always possible.

The authors express their appreciation to S D Ganichev and V V Belkov for their valuable advice. This work was supported by a grant from the Russian Science Foundation, no. 19-12-00034.

References

1. Hsieh D et al. *Nature* **452** 970 (2008)
2. Ganichev S D, Prettl W *J. Phys. Condens. Matter* **15** R935 (2003)
3. Ivchenko E L *Optical Spectroscopy of Semiconductor Nanostructures* (Harrow, UK: Alpha Science, 2005)
4. Ivchenko E L, Pikus G E *JETP Lett.* **27** 604 (1978); *Pis'ma Zh. Eksp. Teor. Fiz.* **27** 640 (1978)
5. Belinicher V I *Phys. Lett. A* **66** 213 (1978)
6. Ganichev S, Prettl W *Intense Terahertz Excitation of Semiconductors* (Oxford: Oxford Univ. Press, 2005) https://doi.org/10.1093/acprof:oso/9780198528302.001.0001
7. Belinicher V I, Sturman B I *Sov. Phys. Usp.* **23** 199 (1980); *Usp. Fiz. Nauk* **130** 415 (1980)
8. Pan Y et al. *Nat. Commun.* **8** 1037 (2017)
9. Olbrich P et al. *Phys. Rev. Lett.* **113** 096601 (2014)
10. Plank H et al. *J. Appl. Phys.* **120** 165301 (2016)
11. Plank H et al. *Phys. Rev. Mater.* **2** 024202 (2018)
12. Plank H, Ganichev S D *Solid-State Electron.* **147** 44 (2018)
13. Danilov S N et al. *Phys. Rev. Appl.* **16** 064030 (2021)
14. Sun X et al. *Sci. Adv.* **7** eabe5748 (2021) https://doi.org/10.1126/sciadv.abe5748

15. Wang Y M et al. *J. Phys. Condens. Matter* **31** 415702 (2019)
16. Ando Y *J. Phys. Soc. Jpn.* **82** 102001 (2013)
17. Zhang H et al. *Nature Phys.* **5** 438 (2009)
18. Xia Y et al. *Nature Phys.* **5** 398 (2009)
19. Chen Y L et al. *Science* **325** 178 (2009)
20. Hsieh D et al. *Phys. Rev. Lett.* **103** 146401 (2009)
21. Bernevig B A, Hughes T L, Zhang S-C *Science* **314** 1757 (2006)
22. Büttner B et al. *Nature Phys.* **7** 418 (2011)
23. Kvon Z D et al. *JETP Lett.* **87** 502 (2008); *Pis'ma Zh. Eksp. Teor. Fiz.* **87** 588 (2008)
24. Brüne C et al. *Phys. Rev. Lett.* **106** 126803 (2011)
25. Dantscher K-M et al. *Phys. Rev. B* **95** 201103 (2017)
26. Dantscher K-M et al. *Phys. Rev. B* **92** 165314 (2015)
27. Candussio S et al. *Phys. Rev. Mater.* **3** 054205 (2019)
28. Hubmann S et al. *Phys. Rev. Mater.* **4** 043607 (2020)
29. Kikoin I K, Noskov M M *Phys. Z. Sowjetunion* **5** 586 (1934); *Zh. Eksp. Teor. Fiz.* **4** 123 (1934)
30. Kikoin I K, Lazarev S D *Sov. Phys. Usp.* **21** 297 (1978); *Usp. Fiz. Nauk* **124** 597 (1978)
31. Galeeva A V et al. *Semicond. Sci. Technol.* **31** 095010 (2016)
32. Egorova S G et al. *Sci. Rep.* **5** 11540 (2015)
33. Galeeva A V et al. *Beilstein J. Nanotechnol.* **8** 167 (2017)
34. Galeeva A V et al. *Nanomaterials* **11** 3207 (2021)
35. Dvoretsky S et al. *J. Electron. Mater.* **39** 918 (2010)
36. Varavin V S et al. *J. Cryst. Growth* **159** 1161 (1996)
37. Rogalski A *Rep. Prog. Phys.* **68** 2267 (2005)
38. Rumyantsev V V et al. *Semiconductors* **47** 1438 (2013); *Fiz. Tekh. Poluprovodn.* **47** 1446 (2013)
39. Kozlov D V et al. *JETP Lett.* **113** 402 (2021); *Pis'ma Zh. Eksp. Teor. Fiz.* **113** 399 (2021)
40. Galeeva A V et al. *JETP Lett.* **106** 162 (2017); *Pis'ma Zh. Eksp. Teor. Fiz.* **106** 156 (2017)
41. Shuvaev A M et al. *Semicond. Sci. Technol.* **27** 124004 (2012)
42. Dziom V et al. *Nat. Commun.* **8** 15197 (2017)
43. Shuvaev A et al. *Appl. Phys. Lett.* **102** 241902 (2013)
44. Shuvaev A M et al. *Phys. Rev. B* **87** 121104 (2013)
45. Brüne C et al. *Phys. Rev. Lett.* **106** 126803 (2011)
46. Olshanetsky E B et al. *JETP Lett.* **93** 526 (2011); *Pis'ma Zh. Eksp. Teor. Fiz.* **93** 584 (2011)
47. Savchenko M L et al. *J. Phys. Condens. Matter* **35** 345302 (2023)
48. Kvon Z D et al. *Phys. Usp.* **63** 629 (2020); *Usp. Fiz. Nauk* **190** 673 (2020)
49. Candussio S et al. *Phys. Rev. Mater.* **3** 054205 (2019)
50. Savchenko M L et al. *Appl. Phys. Lett.* **117** 201103 (2020)
51. Shuvaev A M et al. *Semicond. Sci. Technol.* **27** 124004 (2012)
52. Gospodarič J et al. *Phys. Rev. B* **99** 115130 (2019)
53. Mani R G et al. *Nature* **420** 646 (2002)
54. Tomaka G et al. *Opto-Electron. Rev.* **25** 188 (2017)
55. Galeeva A V et al. *Beilstein J. Nanotechnol.* **9** 1035 (2018)
56. Galeeva A V et al. *Sci. Rep.* **10** 2377 (2020)
57. Galeeva A V et al. *Semiconductors* **54** 1064 (2020); *Fiz. Tekh. Poluprovodn.* **54** 873 (2020)
58. Kazakov A S et al. *JETP Lett.* **112** 246 (2020); *Pis'ma Zh. Eksp. Teor. Fiz.* **112** 263 (2020)
59. Kazakov A S et al. *Sci. Rep.* **11** 1587 (2021)
60. Kazakov A S et al. *JETP Lett.* **113** 542 (2021); *Pis'ma Zh. Eksp. Teor. Fiz.* **113** 548 (2021)
61. Kazakov A S et al. *Sci. Rep.* **11** 11638 (2021)
62. Kazakov A S et al. *Bull. Russ. Acad. Sci. Phys.* **87** 739 (2023); *Izv. Ross. Akad. Nauk. Ser. Fiz.* **87** 843 (2023)
63. Roth A et al. *Science* **325** 294 (2009)